

# Modeling the Imaginary Branch in III-V Tunneling Devices: Effective Mass vs $k \cdot p$

Cem Alper\*, Michele Visciarelli†, Pierpaolo Palestri‡, Jose L. Padilla\*, Antonio Gnudi†, Elena Gnani† and Adrian M. Ionescu\*

\*NANOLAB, Ecole Polytechnique Fédérale de Lausanne, Switzerland

†DEI/ARCES, University of Bologna, Italy

‡DIEGM, University of Udine, Udine 33100, Italy

**Abstract**—In this work we extend an effective mass model for computing the drain current of tunnel-FETs to account for the anti-crossing of the light- and heavy-hole branches of the valence band. The model is validated by comparison with NEGF simulations based on a  $k \cdot p$  Hamiltonian. Application of the new model to the electron-hole bilayer TFET is provided showing that the inclusion of the asymmetry of the real and imaginary branches of the hole dispersion relation is critical in determining the device characteristics.

## I. INTRODUCTION

Recent increase of interest in nanoscale band-to-band tunneling (BTBT) devices such as the Tunnel FET (TFET) has brought in the need for new simulation methods for accurate and efficient simulation of such devices. Most of the approaches employed in the literature are based on full-quantum models with atomistic or  $k \cdot p$  Hamiltonians [1]–[3] which accurately describe the coupling between the valence and conduction bands.

Models based on the effective mass approximation (EMA) are more efficient from a numerical point of view and can handle large device and include phonon assisted tunneling with a small additional effort [4]. They are however based on separate solutions of the electron and hole Schrödinger equations. The coupling between band is added in post processing assuming suitable dispersion relationship in the gap. The "anti-crossing" [5] of the light-hole (LH) and heavy-hole (HH) branches is not natively included in such approaches. With "anti-crossing" we mean that, the top of the valence band in III-V semiconductors is connected with the conduction band through an imaginary branch with low mass (the LH one), even in the presence of strong quantization that makes the HH branch dominate. In fact, NEGF simulations [2] show significant BTBT current even in quantum well and nanowires, where LH are very low in energy. In other words, the tunneling effective mass is closer to the LH mass even when HH subbands are concerned.

*The goal here is to show that the EMA-NP model using the LH mass as tunneling mass for the HH subband fairly reproduces the  $k \cdot p$  results.*

## II. MODEL DESCRIPTION

The simulator employed here relies on the 1D solution of the closed-boundary Schrödinger equation using the EMA [4] with nonparabolicity (NP) corrections [6], [7]. The model has been

originally developed for the electron-hole bilayer Tunnel FET (EHBTFET) [4] but, in order to analyze the anti-crossing in a simpler template structure, it is applied here to quantum-well diodes (Fig. 1), where size-induced quantization takes place in the direction normal to the p-n junction (we have the so-called 2D-2D edge tunneling [8]). The open boundaries along the x-direction are emulated by taking long n and p side regions (100nm each). The direct band-to-band tunneling current is given by [7]:

$$I_D \simeq \frac{4\pi qW}{\hbar} \sum |M_{cv}|^2 JDOS(E) \Theta(E_h - E_e) (f_c - f_v) \quad (1)$$

where  $f_c$  and  $f_v$  are the Fermi distributions of the electrons and holes respectively,  $E_e$  and  $E_h$  are the quantized energies for electron and hole states respectively.  $\Theta(E_h - E_e)$  is the step function denoting the alignment of the quantized subband energies.  $|M_{cv}|^2$  is the squared magnitude of the coupling element between the electron and hole states, given as [9]:

$$M_{cv} = q \sqrt{\frac{\hbar^2}{4mE_G}} \delta_{k_\perp, k'_\perp} \int \psi_{k'\alpha'}^*(x) |F(x)| \psi_{k\Gamma}(x) dx \quad (2)$$

where  $|F(x)|$  is the magnitude of the electric field,  $\psi_{k'\alpha'}$  and  $\psi_{k\Gamma}$  are the wavefunctions for the hole and electron states respectively. From this expression it is obvious that spatial overlap of the WFs critically determine the coupling strength between the electron and hole states and therefore the BTBT current.

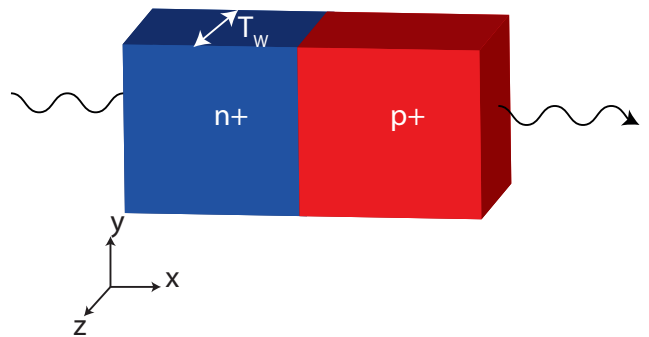


Fig. 1. Sketch of the InAs quantum well diode as a 2D-2D edge tunneling device.

Compared to the bulk case with no quantization, incorporating quantization effects to simulate the quantum well diode structure requires two modifications. The first modification is the use of the 1-D joint density of states (compared to the 2D one used in bulk diodes) JDOS(E) which preserves the  $k$  along the  $y$  direction only, since the  $k$ -space is unconstrained along  $y$  [4]. The second modification is the rigid shift of the bulk band edges according to the quantized energy levels along the  $z$  direction. Quantized energy levels are calculated numerically using the 4-band  $k \cdot p$  simulator [3]. The potential is assumed to be uniform in the transverse ( $y$ ) direction.

To obtain the tunneling parameters, we have fitted the imaginary dispersion relation (see Fig. 2 for the real and imaginary dispersion relations obtained) from the 4-band  $k \cdot p$  simulator [3]. The effective masses obtained from the fitting are reported in Tab. I. For InAs, the fitted tunneling effective mass ( $m_{HH,imag}^*$ ) is drastically different than the effective mass of the real branch ( $m_{HH}^*$ ). Note that the fitted value almost coincides with the bulk LH mass, thus confirming the results of [10] and highlighting the anti-crossing [5]. The electron dispersion, on the other hand, rather exhibits a symmetry between the real and imaginary branches.

TABLE I  
EFFECTIVE MASSES AND CONDUCTION BAND NONPARABOLICITY FACTOR EXTRACTED FOR INAS SLABS OF DIFFERENT THICKNESSES (SEE FIG. 2)

Slab thickness	$m_{HH,real}^*$	$m_{HH,imag}^*$	$m_e^*$	$\alpha$ [eV $^{-1}$ ]
5nm	0.33	0.037	0.037	3.6
10nm	0.33	0.03	0.026	
15nm	0.33	0.023	0.025	

This finding, however, brings up the question of using adequate effective masses for the classically allowed ( $E_h < E_V$ ) and forbidden regions ( $E_h > E_V$ ), since the effective mass in the forbidden region strongly determines the amplitude of the wavefunction tail, and therefore the spatial overlap between the electron and hole states in the bandgap (eq. 2). To overcome this issue, we utilize the WKB approximation using single-band approximation, in which we modify the effective mass in the forbidden region with the value extracted from the imaginary dispersion calculated by the 4-band  $k \cdot p$  simulator (table I). The WF is then calculated using the familiar expressions given by the WKB approximation [12]:

$$\psi_h(x) = \begin{cases} \frac{C}{\sqrt{|k_x(x)|}} e^{-i \int k_x(x) dx} & E_h < E_V \\ \frac{C}{\sqrt{|k_x(x)|}} e^{-\int |k_x(x)| dx} & E_h > E_V \end{cases} \quad (3)$$

where  $C$  is the normalization constant.

For all the results presented here, we take the potential profile calculated by the  $k \cdot p$  simulator as input and run the model as a post-processing step, in order to isolate the influence of the tunneling parameters from the influence of device electrostatics.

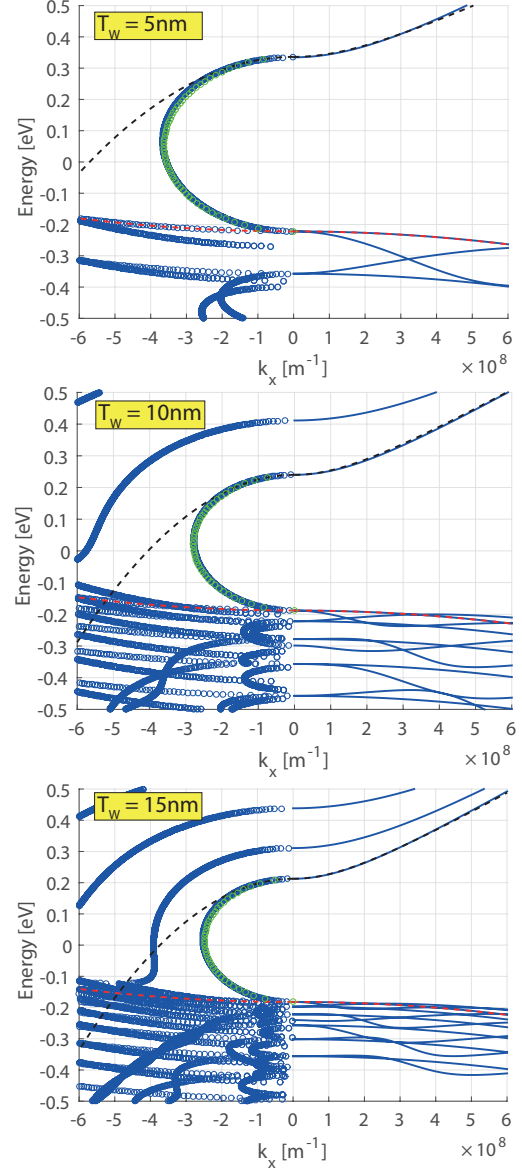


Fig. 2. Real ( $k_x > 0$ ) and imaginary ( $k_x < 0$ ) dispersion for (up) 5nm (middle) 10nm (bottom) 15nm thick InAs from  $k \cdot p$ . The red and black curves indicate the real and imaginary relations predicted by single band approximation for HH (with mass  $m_{HH,real}^*$ ) and conduction band (with mass  $m_e^*$ ), respectively. The green curve is the fit obtained by the Kane's two-band dispersion relation [11] ( $\kappa = \frac{1}{\hbar} \sqrt{m_r E_G^T (1 - \alpha^2)}$  with  $\alpha = -\frac{m_0}{2m_r} + 2\sqrt{\frac{m_0}{2m_r} \left( \frac{E - E_V}{E_G^T} - \frac{1}{2} + \frac{m_0^2}{16m_r^2} + \frac{1}{4} \right)}$  and  $\frac{1}{m_r} = \frac{1}{m_{HH,imag}} + \frac{1}{m_e}$ ). Parameters from the fitting are given in Table I.

### III. RESULTS & DISCUSSION

Fig. 3 shows the current densities obtained by the EMA-NP model for a bulk diode ( $T_W = 50$ nm) with different doping levels. A general agreement with the  $k \cdot p$  results, better at low doping levels, is observed.

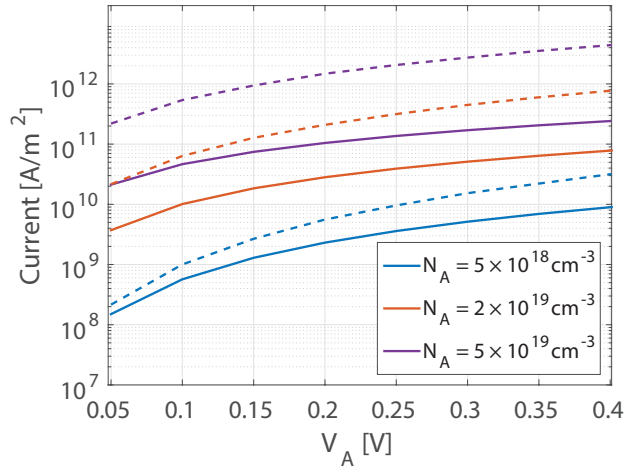


Fig. 3. I-V characteristics of bulk diodes from EMA-NP (dashed) and  $k \cdot p$  (solid) for various doping levels.

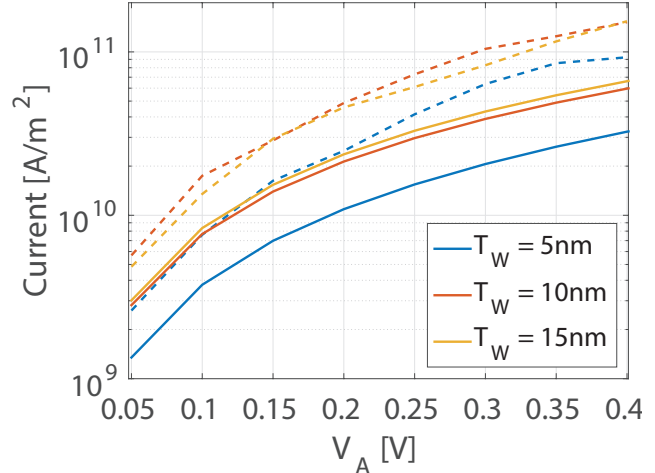


Fig. 5. Same as Fig. 4 but for various  $T_W$  values.  $N_A = 2 \times 10^{19} \text{cm}^{-3}$ .

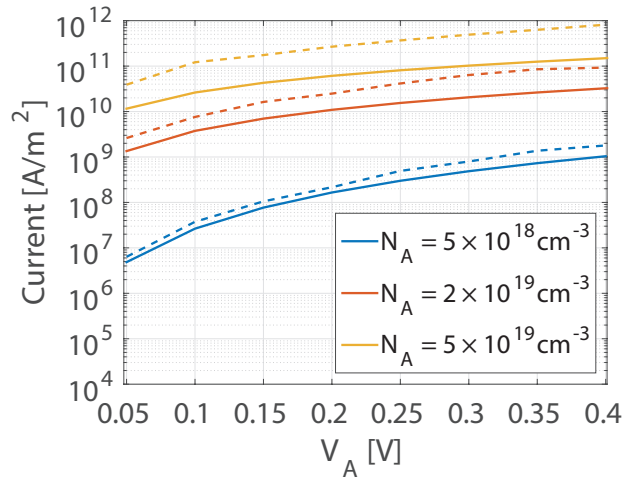


Fig. 4. Comparison of I-V characteristics for the QW diode shown in Fig. 1 considering various doping levels.  $T_W = 5\text{nm}$ . EMA-NP (dashed),  $k \cdot p$  (solid).

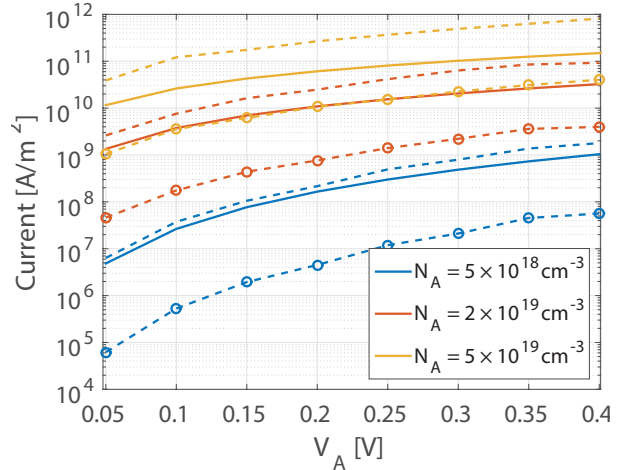


Fig. 6. Comparison of I-V characteristics using  $k \cdot p$  (solid) and EMA-NP with  $m_{tun,HH} = 0.03m_0$  (Dashed) or with  $m_{tun,HH} = 0.33m_0$  (Dashed with symbols).

Fig. 4 compares the  $k \cdot p$  and EMA-NP results for QW diodes (Fig. 1) with  $T_W = 5\text{nm}$  and different doping levels. The difference between the models seems to be increasing with increasing doping levels, which results from higher  $k$ -states being able to contribute to the current, where the EMA description starts to break down.

Fig. 5 compares the models for different  $T_W$ : both models show the same trend of current increase as  $T_W$  increases. However, comparing Figs. 3 & 4, it is seen that the current density remains approximately the same, which signals that in both QW and bulk diodes, it is the same imaginary path that is connecting the valence and conduction bands with very similar effective mass values.

To assess the impact of the large asymmetry in mass of the real and imaginary branches, we compare the cases using the

real or imaginary branch masses in the forbidden region: Fig. 6, shows a dramatic decrease in current when the HH mass is used for tunneling.

Fig. 8 presents an application of the model to the EHBTFET (sketched in Fig. 7), a 2D-2D face tunneling [8] device which utilizes BTBT between quantized 2D electron and hole gases. [4]. The I-V characteristics given in Fig. 8 demonstrate the importance of using the correct tunneling mass in the simulations. About one order of magnitude of increase in the tunneling current is seen when using the LH mass for tunneling, since it allows for much higher spatial overlap between wavefunctions [4].

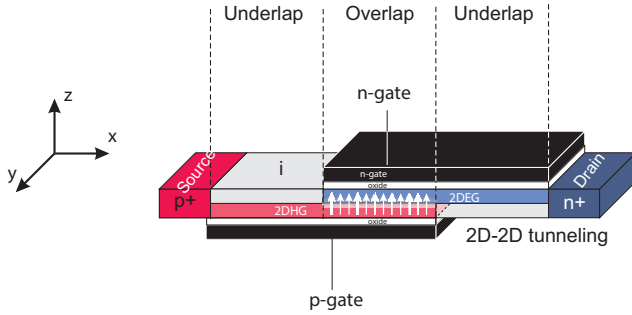


Fig. 7. Sketch of the InAs EHBTFET device structure and indication of 2D-2D subband-to-subband tunneling.  $L_{\text{OVERLAP}} = 50\text{nm}$ ,  $T_{\text{OX,EOT}} = 0.5\text{nm}$ ,  $T_{\text{CH}} = 10\text{nm}$ ,  $L_{\text{UNDERLAP}} = 50\text{nm}$ .

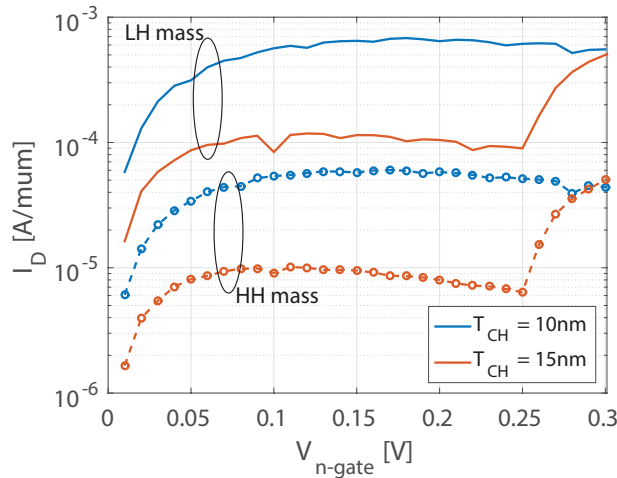


Fig. 8. Transfer characteristics of the InAs EHBTFET of Fig. 7 using HH mass (dashed w/symbols) or calibrated effective mass of the imaginary branch (solid) for tunneling. The effective mass values used for simulations with different channel thicknesses are given in Table I.  $V_{\text{p-gate}} = -V_{\text{n-gate}}$ .  $V_{\text{DS}} = 0.3\text{V}$ .

#### IV. CONCLUSION

A EMA-NP model has been modified to account for anti-crossing of the valence band and transverse quantization through adequate shifting of energy bands and modification of the transverse JDOS. A general agreement is observed between the EMA-NP and  $k \cdot p$  models after proper calibration. EHBTFET simulations indicate that asymmetry of the effective masses of the imaginary and real branches of the hole subbands has a drastic impact on the ON current levels, making it essential to include this effect in the simulations.

#### ACKNOWLEDGMENT

The research leading to these results has received funding from the European Community's Seventh Framework Programme under grant agreement No. 619509 (Project E2-Switch).

#### REFERENCES

- [1] M. Luisier, A. Schenk, W. Fichtner, and G. Klimeck, "Atomistic simulation of nanowires in the  $sp^3d^5s^*$  tight-binding formalism: From boundary conditions to strain calculations," *Physical Review B*, vol. 74, p. 205323, Nov. 2006.
- [2] F. Conzatti, M. G. Pala, D. Esseni, E. Bano, and L. Selmi, "Strain-induced performance improvements in InAs nanowire tunnel FETs," *IEEE Transactions on Electron Devices*, vol. 59, no. 8, pp. 2085–2092, 2012.
- [3] E. Baravelli, E. Gnani, R. Grassi, A. Gnudi, S. Reggiani, and G. Bacarani, "Optimization of n- and p-type TFETs integrated on the same InAs/ $\text{Al}_x\text{Ga}_{1-x}\text{Sb}$  technology platform," *IEEE Transactions on Electron Devices*, vol. 61, pp. 178–185, Jan. 2014.
- [4] C. Alper, L. Lattanzio, L. De Michielis, P. Palestri, L. Selmi, and A. M. Ionescu, "Quantum Mechanical Study of the Germanium Electron Hole Bilayer Tunnel FET," *IEEE Transactions on Electron Devices*, vol. 60, pp. 2754–2760, Sept. 2013.
- [5] S. Jin, A.-t. Pham, Woosung Choi, Y. Nishizawa, Young-Tae Kim, Keun-Ho Lee, Youngkwan Park, and Eun Seung Jung, "Performance evaluation of InGaAs, Si, and Ge nFinFETs based on coupled 3D drift-diffusion/multisubband boltzmann transport equations solver," in *2014 IEEE International Electron Devices Meeting*, pp. 7.5.1–7.5.4, 2014.
- [6] C. Troger, H. Kosina, and S. Selberherr, "Modeling nonparabolicity effects in silicon inversion layers," in *SISPAD '97. 1997 International Conference on Simulation of Semiconductor Processes and Devices. Technical Digest*, pp. 323–326, Ieee, 1997.
- [7] C. Alper, P. Palestri, J. L. Padilla, A. Gnudi, R. Grassi, E. Gnani, M. Luisier, and A. M. Ionescu, "Efficient quantum mechanical simulation of band-to-band tunneling," in *EUROSOL-ULIS 2015: 2015 Joint International EUROSOL Workshop and International Conference on Ultimate Integration on Silicon*, pp. 141–144, 2015.
- [8] S. Agarwal and E. Yablonovitch, "Pronounced Effect of pn-Junction Dimensionality on Tunnel Switch Threshold Shape," *Mesoscale and Nanoscale Physics*, vol. 46, pp. fmiii–fmiv, Sept. 2011.
- [9] A. Schenk, M. Stahl, and H.-J. Wünsche, "Calculation of Interband Tunneling in Inhomogeneous Fields," *physica status solidi (b)*, vol. 154, pp. 815–826, Aug. 1989.
- [10] A. Pan and C. O. Chui, "Modeling direct interband tunneling. II. Lower-dimensional structures," *Journal of Applied Physics*, vol. 116, p. 054509, Aug. 2014.
- [11] E. O. Kane, "Theory of Tunneling," *Journal of Applied Physics*, vol. 32, no. 1, p. 83, 1961.
- [12] D. J. Griffiths, *Introduction to Quantum Mechanics (Second Edition)*. Pearson Education International, 2005.